# Transduction of High-Frequency Micromechanical Resonators Using Depletion Forces in p-n Diodes

Eugene Hwang, *Student Member, IEEE*, and Sunil A. Bhave, *Senior Member, IEEE*

***Abstract*—We present in this paper the design and fabrication of a homogeneous silicon micromechanical resonator actuated using forces acting on the immobile charge in the depletion region of a symmetrically doped p-n diode. The proposed resonator combines the high quality factor $Q$ of air-gap-transduced resonators with the frequency-scaling benefits of internal dielectrically transduced resonators. Using this transduction method, we demonstrate a thickness-longitudinal-mode micromechanical resonator with $Q \sim 18000$ at a resonant frequency of 3.72 GHz at room temperature, yielding an $f \cdot Q$ product of 6.69 $\times$ $10^{13}$ Hz, which is the highest reported value for a silicon micromechanical resonator to date.**

***Index Terms*—Micromechanical resonators, p-n diode, quality factor $(Q)$, radio-frequency microelectromechanical systems (RF MEMS).**

## I. Introduction

THE potential of micromechanical devices as resonators with high quality factor $Q$ has been recognized since the seminal paper by Nathanson *et al.* describing the resonant gate transistor [1]. Since new developments in the areas of surface and bulk micromachining ushered in and established the field now known as microelectromechanical systems (MEMS), a variety of micromechanical resonator designs have been developed, ranging from flexural-mode cantilevers and clamped beam resonators [2], [3] to bulk-acoustic-mode resonators [4]–[6]. Such resonators are finding use in a variety of systems from chemical sensing [7] to high-precision oscillators [8]. Continued research has pushed steadily the resonant frequencies of these devices into the multigigahertz range while improving transduction efficiency and reducing motional impedance, which is the ratio of the actuation input voltage to the transduced output current and is a metric of the overall efficiency of the resonator. Recent developments have included fabrication techniques to create large aspect-ratio resonators by minimizing the gap width and maximizing the transduction area of air-gap-transduced silicon resonators [5], [9], [10] or using different transducer (capacitive or piezoelectric) materials in a composite resonator structure [6], [11], [12]. While these methods show promise for increasing the transduction efficiency, there are certain limitations associated with each. High-aspect-ratio air-gap resonators have the potential for high $Q$ due to their homogeneous resonator structure but are limited due to high motional impedance in addition to low fabrication yield and reliability. Piezoelectric transducers [11] have demonstrated low motional impedances, but the greater inherent material losses compared with silicon limit the quality factor of these devices. The use of high-$k$ dielectrics [6], [12], [13] increases the transduction efficiency over air-gap-transduced resonators by bolstering the dielectric constant of the capacitive transducer and has the added benefit of increased reliability, but interface losses between the resonator body and transducer materials, particularly when the transducer is placed at locations of maximum strain, limit the $Q$ of these devices.

In this paper, we present a method of transduction that combines the strengths of the previously mentioned methods to design high-$Q$ resonators at gigahertz frequencies. This is done by actuating mechanical motion using the force acting on the immobile charge within the depletion region of a p-n diode. Similar depletion-layer actuation has been observed with atomic force microscopy using gold–silicon Schottky diodes to excite resonance in cantilever beams [14] and to study electrostriction in silicon [15] at low frequencies. Due to the internal nature of depletion-layer transduction (i.e., the force is applied within the resonator), such resonators can be actuated efficiently at high frequencies when the junction is placed at optimal locations within the resonator. In this paper, we present a detailed theory of operation for the p-n-diode-transduced micromechanical resonators, which include some subtle but important differences with typical capacitive transduction, and show experimental results for thickness-longitudinal-mode resonators (see Fig. 1) to validate our claims. After a discussion of these results, we conclude with the implications of this paper.

## II. Theory of Operation

### A. Actuation

This paper combines the theories of depletion-layer actuation [14] and internal dielectric transduction [6]. We first find the force distribution within the resonator body. This force distribution arises from the electrostatic force acting on the immobile charge (i.e., donor/acceptor ions) within the depletion region of the p-n junction. This is shown graphically in Fig. 2. Assuming an abrupt symmetric junction profile, the expressions for the

Manuscript received February 2, 2011; revised April 19, 2011; accepted May 16, 2011. Date of publication June 23, 2011; date of current version July 22, 2011. This work was supported in part by the Defense Advanced Research Projects Agency as part of the Hybrid-Insect MEMS program and through Army Research Labs. The review of this paper was arranged by Editor A. M. Ionescu.

The authors are with the School of Electrical and Computer Engineering at Cornell University, Ithaca, NY 14853 USA (e-mail: eoh3@cornell.edu; sunil@ece.cornell.edu).

Color versions of one or more of the figures in this paper are available online at http://ieeexplore.ieee.org.

Digital Object Identifier 10.1109/TED.2011.2158103

0018-9383/$26.00 © 2011 IEEE

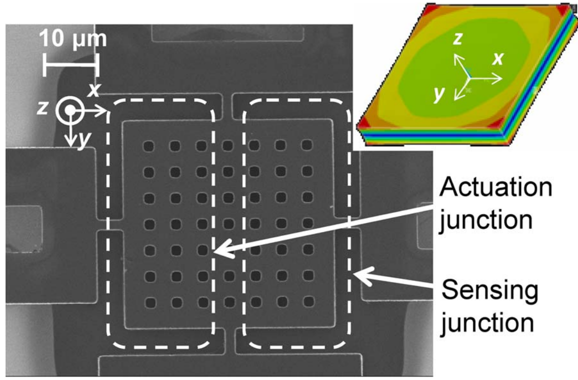


Fig. 1. Scanning-electron-microscopic image of the 40 $\mu m \times 40$ $\mu m$ p-n-diode-transduced micromechanical resonator. The resonant frequency of 3.72 GHz is determined by the silicon device layer thickness (no electrodes or other mass loading layers). The displacement amplitude in the thickness direction of the resonant mode shape is shown in the inset plot. Etch holes are required for timed HF release.

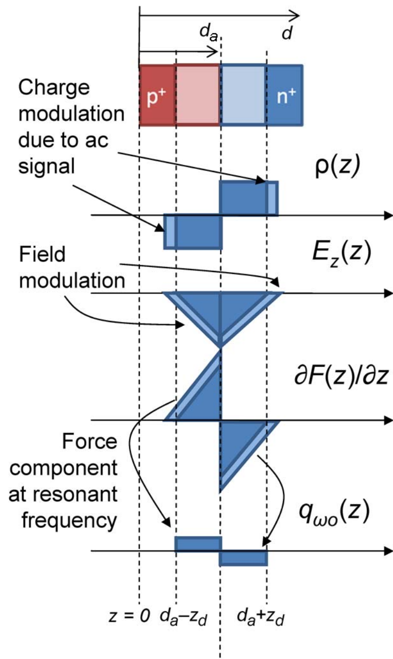


Fig. 2. Illustration of the principle of actuation in the input junction showing the charge density $\rho$, the electric field in the thickness direction $E_z$, and the force component at the resonant frequency $q_{\omega o}$ throughout the structure.

charge distribution $\rho(z)$, the electric field $E_z(z)$, and the force distribution $\partial F/\partial z$ are given by

$$\rho(z) = \begin{cases} -eN, & d_a - z_d < z < d_a \\ eN, & d_a < z < d_a + z_d \end{cases} \quad (1)$$

$$E_z(z) = \begin{cases} -\frac{eN}{\varepsilon_{\rm si}\varepsilon_0}(z_d - d_a + z), & d_a - z_d < z < d_a \\ \frac{eN}{\varepsilon_{\rm si}\varepsilon_0}(z - z_d - d_a), & d_a < z < d_a + z_d \end{cases} \quad (2)$$

$$\frac{\partial F}{\partial z} = \begin{cases} \frac{e^2N^2A_j}{\varepsilon_{\rm si}\varepsilon_0}(z + z_d - d_a), & d_a - z_d < z < d_a \\ \frac{e^2N^2A_j}{\varepsilon_{\rm si}\varepsilon_0}(z - z_d - d_a), & d_a < z < d_a + z_d \end{cases} \quad (3)$$

where $e$ is the elementary charge, $N$ is the symmetric doping concentration, $\varepsilon_{\rm si}$ is the relative permittivity of silicon, $\varepsilon_0$ is the permittivity of free space, $A_j$ is the junction area, and $2z_d$ is the junction depletion width given by

$$z_d(v_{\rm in}) = \sqrt{\frac{\varepsilon_{\rm si}\varepsilon_o}{eN}\left(\phi_{\rm bi} - (V_{\rm DC} + v_{\rm in}(t))\right)} \quad (4)$$

where $\Phi_{\rm bi}$ is the junction built-in voltage.

Equations (1)–(4) indicate that this function is nonlinear with the input excitation voltage described by $v_{\rm in} = v_o e^{-j\omega_o t}$. If $v_o \ll \Phi_{\rm bi} - V_{\rm DC}$, then (3) can be linearized around the bias point, yielding the distributed force at the excitation frequency as follows:

$$q_{\omega_o}(z, t) \approx \begin{cases} -\frac{(eN)^{3/2}A_j}{2\sqrt{\varepsilon_{\rm si}\varepsilon_o(\phi_{\rm bi}-V_{\rm DC})}}v_{\rm in}, & d_a - z_d \le z < d_a \\ \frac{(eN)^{3/2}A_j}{2\sqrt{\varepsilon_{\rm si}\varepsilon_o(\phi_{\rm bi}-V_{\rm DC})}}v_{\rm in}, & d_a < z \le d_a + z_d. \end{cases} \quad (5)$$

This force distribution yields the following equation of motion:

$$\rho A\frac{\partial^2 u}{\partial t^2} - bA\frac{\partial^3 u}{\partial t \partial z^2} - EA\frac{\partial^2 u}{\partial z^2} = q_{\omega_o}(z, t). \quad (6)$$

Here, $\rho$ is the mass density, $E$ is the Young's Modulus, $b$ is the loss factor, $d_a$ is the location of the actuation junction, $A$ is the resonator cross-sectional area, and $u(z, t)$ is the displacement field within the resonator. This field can be written as $u(z, t) = U_o\cos(n\pi z/d)e^{-j\omega_o t}$. Note that from this point forward, the subscripts "$a$" and "$s$" after a comma are used to differentiate between the parameters of the actuation and sensing junctions, respectively. Multiplying (6) by the mode shape and integrating over the thickness $d$ of the resonator allow us to find both the resonant displacement amplitude $U_o$ and the electromechanical transduction efficiency of the actuation junction $\eta_a$, which is the ratio of force applied to the structure over input voltage amplitude given by

$$\eta_a = \frac{2dA_{j,a}}{n\pi}\frac{eN_a}{z_{d0,a}}\sin\left(\frac{n\pi d_a}{d}\right)\sin^2\left(\frac{n\pi}{d}\frac{z_{d0,a}}{2}\right) \quad (7)$$

where $z_{d0,a} = z_{d,a}(v_{\rm in} = 0)$. The resonant displacement amplitude is given by

$$|U_o| = \frac{4Qd^2}{n^3\pi^3 E}\frac{eN_a}{z_{d0,a}}\sin\left(\frac{n\pi d_a}{d}\right)\sin^2\left(\frac{n\pi}{d}\frac{z_{d0,a}}{2}\right)v_{\rm in} \quad (8)$$

where $Q$ is the resonator quality factor and $n$ is the mode number of the thickness longitudinal mode that is excited.

It should be noted that this analysis assumes that the movement of charge at the edges of the depletion region is dominated by the response of majority carriers, i.e., the junction is in reverse bias. This is because the movement of minority carriers is too slow to respond adequately to input voltages at high frequencies. To analyze the behavior in forward bias, an equivalent shunt conductance can be added to model the minority-carrier response time as an RC time constant if necessary. This, however, will not be considered here.

### B. Sensing

The sensing mechanism employed in these devices is described best by the two-port capacitive-sensing scheme

commonly used in electrostatically excited MEMS resonators [4], [5]. This scheme requires a time-varying capacitance at the output, which results in an output current that is transferred to some load, typically a 50-Ω termination for RF measurements. In practical systems, to maximize signal output, this load may be the input of a low-input-impedance amplifier such as a common-gate CMOS amplifier or a shunt feedback operational amplifier. The required time-varying capacitance arises as a result of the mechanical motion of the resonator. When the voltage across the output capacitor is constant, a motional current is produced with magnitude given by $i_m = V_{\mathrm{DC}}(\partial C_{\mathrm{out}}/\partial t)$.

This scenario, however, is exact only in the case when there is a physical separation (i.e., dielectric layer) across which charge is accumulated. This is not exactly the case for the proposed device, which has a depletion layer across which charge can still move. This subtlety complicates the analysis but still results in a model that is mathematically consistent with the simplified capacitive-sensing model. We will present first the simplified calculations and then explore the subtleties that exist for the proposed device.

*Simplified Model:* Assuming that the depletion capacitance at the output behaves like a physical capacitance, the expression for motional current given previously will be valid. Specifically

$$i_m = V_{j,s}\frac{\partial C_{j,s}}{\partial t} = (\Phi_{\mathrm{bi},s} - V_{\mathrm{DC},s}) \times \frac{\partial}{\partial t}\left(\frac{\varepsilon_{\mathrm{si}}\varepsilon_0 A_{j,s}}{2z_{d0,s} - (u(d_s - z_{d0,s}, t) - u(d_s + z_{d0,s}, t))}\right). \quad (9)$$

Simplifying this expression results in

$$i_m = \frac{\omega_o \varepsilon_{\mathrm{si}}\varepsilon_o(\phi_{\mathrm{bi},s} - V_{\mathrm{DC},s})A_{j,s}}{2z_{d0,s}^2} U_o \sin\left(\frac{n\pi z_{d0,s}}{d}\right)\sin\left(\frac{n\pi d_s}{d}\right). \quad (10)$$

As for the case of the actuation junction, an electromechanical transduction efficiency of the sensing junction $\eta_s$ can also be defined as

$$\eta_s = \frac{\varepsilon_{\mathrm{si}}\varepsilon_o(\phi_{\mathrm{bi},s} - V_{\mathrm{DC},s})A_{j,s}}{2z_{d0,s}^2}\sin\left(\frac{n\pi z_{d0,s}}{d}\right)\sin\left(\frac{n\pi d_s}{d}\right). \quad (11)$$

Here, the sensing transducer efficiency is the ratio of the output current over the maximum particle velocity in the resonator.

Again, as in the theory of actuation, this analysis assumes that the distribution of free carriers at the edges of the depletion region responds instantaneously to changes in the capacitance, which would indeed be the case for a physical capacitance. Similarly, this requires the junction to be reverse biased.

*Detailed Analysis:* As previously mentioned, the analysis of the previous subsection is not entirely correct since it is based on a model assuming a physical capacitance. In order to fully analyze this device, we must consider the movement of charge across the junction. For this analysis, we will assume again the instantaneous response of free carriers to the input stimulus (in this case the stress), allowing us to consider this as an adiabatic system. In addition, we will assume that the voltage across the junction is held constant at value $V$. By observing how the stress changes the immobile-charge density and thus the diffusion and drift current components across the junction, we will find an expression for the output motional current.

We start by considering the case of compressive stress, where the silicon lattice is squeezed. A qualitative picture of the process is shown in Fig. 3. Fig. 3(a) shows the band diagram of the initial unstrained junction. All four current components are annotated in this diagram. As shown in the diagram, $J_{n,\mathrm{drift}}$ and $J_{p,\mathrm{drift}}$ are the current components resulting from the movement of thermally generated minority carriers on each side within the diffusion length of the depletion-region edge. These carriers then drift across the junction due to the electric field. There also exist $J_{n,\mathrm{diff}}$ and $J_{p,\mathrm{diff}}$, which are the current components that arise as a result of majority carriers on each side that overcome the potential barrier and diffuse across the junction. These carriers become minority carriers and recombine on the other side of the junction.

When the stress is applied, the immobile-charge density now changes. Since we are considering what happens adiabatically, we can imagine that at the exact moment that the strain compresses the junction, the free carriers have not yet responded. Thus, the depletion-region width initially stays constant, but because of the underlying compression of the ions in the lattice, we expect the charge density and, subsequently, the electric field to now increase within the depletion region. This will increase the barrier height to value $V'$, as indicated by the dashed line in Fig. 3(b). As the barrier increases, $J_{n,\mathrm{drift}}$ and $J_{p,\mathrm{drift}}$ also increase, resulting in a negative current across the junction. Once these minority carriers cross the junction, they become majority carriers, which define the depletion-region width. At this moment, if the potential across the junction were allowed to vary, then the compressive stress would simply increase the effective doping density, and the depletion-region width would remain constant. The total static current across the junction would be the quantity that increases. However, this is where the fact that the potential across the junction is forced constant by a voltage source that becomes important. In this case, the system will try to restore the barrier height to $V$, and the increased negative currents would allow this to happen by using the newly available majority carriers to decrease the depletion-region width and thus, the electric field. When the barrier height is restored to $V$, the currents will return to the original value expected for the corresponding bias. In contrast to the case where the potential were allowed to vary freely, the quantity that permanently changes is now the depletion-region width.

The case of tensile strain is exactly the opposite in that the immobile-charge density effectively decreases, resulting in a decrease in the barrier height and, thus, an increase in the $J_{n,\mathrm{diff}}$ and $J_{p,\mathrm{diff}}$ components. Again, since the voltage across the junction is held constant, the movement of charge provides a means for the system to readjust the depletion width to return to the original potential. This process is not illustrated here for the sake of brevity.

We can analyze quantitatively the effect of strain on the change in depletion width by considering the amount of immobile charge within the depletion region and by finding how much this width must change in order to accommodate the

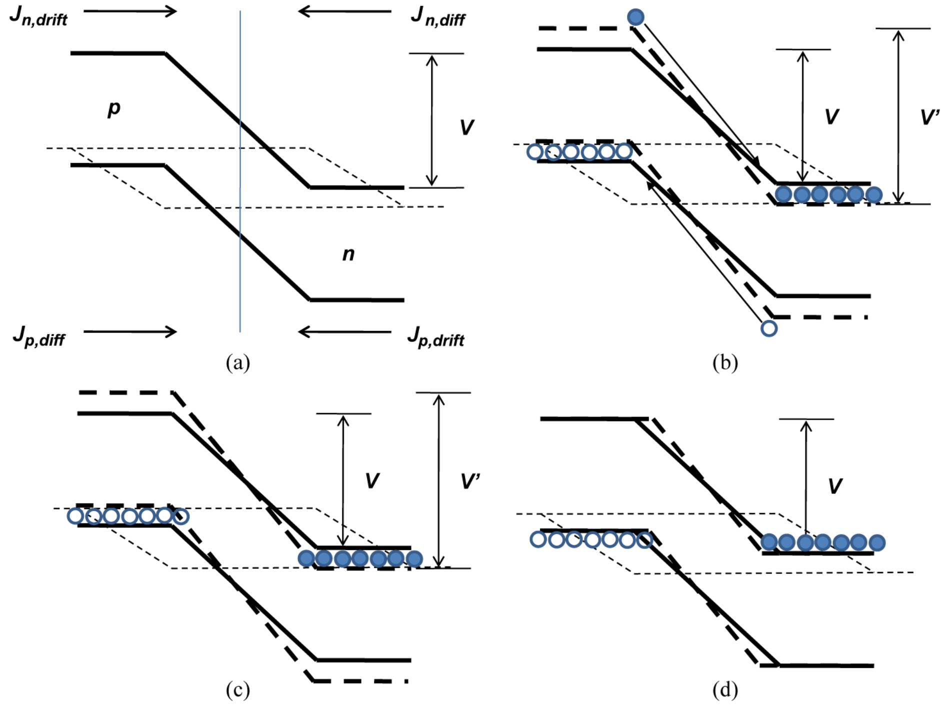


Fig. 3. (a) Band diagram of the unstrained p-n junction showing individual current components. (b) Compressive strain in the junction causes an increase in the dopant density, subsequently increasing the electric field and the barrier height. This causes the current components $J_{n,\,\mathrm{drift}}$, $J_{p,\,\mathrm{drift}}$ to increase while decreasing $J_{n,\,\mathrm{diff}}$, $J_{p,\,\mathrm{diff}}$. The result is a net movement of electrons to the n-side and holes to the p-side. (c) Excess carriers become majority carriers when they cross the junction. (d) These carriers subsequently return the system to the original barrier height.

same voltage. First, we must consider how the strain changes the immobile-charge density. If we consider the infinitesimal section of the depletion region $dz$ and the charge within this region $dQ$, we can observe that

$$dz' = dz\,(1+\varepsilon(z))\,, dQ = eN_{\mathrm{so}}A_{j,\,s}dz = eN_s(z)A_{j,\,s}dz' \tag{12}$$

$$\Rightarrow N_s(z) = \frac{N_{\mathrm{so}}}{1+\varepsilon(z)} \approx N_{\mathrm{so}}\,(1-\varepsilon(z)) \tag{13}$$

where $\varepsilon(z)$ is the strain and $N_{\mathrm{so}}$ is the doping density, i.e., the original immobile-charge density. The last simplification is made possible by assuming a small strain $(\varepsilon(z) \ll 1)$ value.

The total potential across the unstrained junction is given by the following expression:

$$V = \int_{-z_{d,\,s}}^{+z_{d,\,s}} \vec{E}_z \bullet d\vec{l} \tag{14}$$

where the electric field is given by

$$E_z = \begin{cases} -\frac{eN_{\mathrm{so}}}{\varepsilon_{\mathrm{si}}\varepsilon_o}(z_{d,\,s} - d_s + z), \; d_s - z_{d,\,s} \le z < d_s \\ \frac{eN_{\mathrm{so}}}{\varepsilon_{\mathrm{si}}\varepsilon_o}(z - z_{d,\,s} - d_s), \; d_s < z \le d_s + z_{d,\,s}. \end{cases} \tag{15}$$

Likewise, the potential across a strained junction is given by

$$V = \int_{-z'_{d,\,s}}^{+z'_{d,\,s}} \vec{E}_{z,\,\mathrm{strained}} \bullet d\vec{l} \tag{16}$$

and in this case, $E_{z,\mathrm{strained}}$ is equivalent to (15) with $N_{\mathrm{so}}$ replaced by $N_s(z)$ and $z_{d,\,s}$ replaced by the new strained depletion width $z'_{d,\,s}$. Since the potential across both the unstrained and strained junctions must be equal, we can then set (14) and (16) equal and solve for $z'_{d,\,s}$ in terms of $z_{d,\,s}$. If we assume that the maximum displacement amplitude is much less than the wavelength (i.e., $\varepsilon(z) \ll \lambda/d$), then we obtain the rather interesting result that

$$z'_{d,\,s} \approx z_{d,\,s}\,(1 + \varepsilon(z_{d,\,s}))\,. \tag{17}$$

This expression for $z'_{d,\,s}$ indicates that the new depletion width is just the original depletion width changed by the amount of strain at the depletion-width edge. In other words, we can think of the edges of the depletion width mimicking the movement of the charge accumulation layers (i.e., capacitor plates) of a physical capacitor. This result justifies the use of the simplified model previously mentioned for the case of reverse bias and small strain, allowing easy modeling of the proposed resonator.

*Equivalent Circuit Model:* To incorporate more readily the behavior of the p-n-diode resonator into other electrical systems, we can define an equivalent Butterworth–Van Dyke (BVD) circuit model to describe its resonant behavior, as shown in Fig. 4. The expressions for the motional impedance, motional inductance, and motional capacitance are well known and can be defined in terms of previously defined parameters as follows:

$$R_x = \frac{n\pi A\sqrt{E\rho}}{2Q}\frac{1}{\eta_a\eta_s}, L_x = \frac{\rho A d}{2}\frac{1}{\eta_a\eta_s}, C_x = \frac{2d}{n^2\pi^2 EA}\eta_a\eta_s. \tag{18}$$

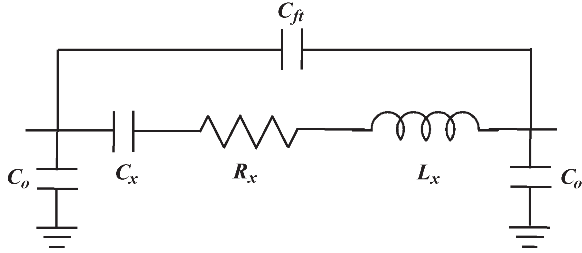


Fig. 4. Equivalent BVD circuit model of the proposed p-n-diode resonator in a two-port configuration.

In addition to these series-resonant circuit components, there are also two shunt capacitors at the input and the output, which are equivalent to the junction depletion capacitances as follows:

$$C_{o,a} = \sqrt{\frac{\varepsilon_{\rm si}\varepsilon_0 e N_a A_{j,a}}{4\left(\Phi_{{\rm bi},a} - V_{{\rm DC},a}\right)}} C_{o,s} = \sqrt{\frac{\varepsilon_{\rm si}\varepsilon_0 e N_s A_{j,s}}{4\left(\Phi_{{\rm bi},s} - V_{{\rm DC},s}\right)}}. \tag{19}$$

Using this BVD model allows for an easy simulation of the resonator in conventional circuit simulators, greatly simplifying the design of oscillators and filters using these devices.

*Effects of Asymmetric Doping:* In conventional semiconductor processes, it is difficult to achieve perfectly symmetric doping profiles, particularly for the high doping concentrations required for efficient transduction in the proposed device. This doping asymmetry will have undoubtedly some effect on the transduction efficiency of the p-n-diode-transduced resonators. A detailed analysis will be omitted for brevity, but a look in Fig. 2 illustrates what will happen as the doping level becomes more and more asymmetric. As the doping asymmetry increases, the charge density, the electric field, and the force distribution will all approach a very tall and thin distribution in the highly doped semiconductor, whereas the depletion region will extend far into the lightly doped semiconductor. In the extreme case of a Schottky junction, the result will be an almost delta-function force distribution exactly at the metallurgical junction. For such a junction, the optimal junction location will now be at a displacement maxima (i.e., edges of the resonator for the current device), and even at the optimal junction location, the efficiency will be decreased. Furthermore, the benefits associated with internal transduction will no longer be seen since the force distribution looks much like that of an externally transduced air-gap resonator. However, this is only in the case of extremely asymmetric doping; for the doping asymmetries that can be achieved through careful process characterization, the overall effect will be a slight reduction in transducer efficiency and a shift of the optimal junction location. Our results will show that although asymmetric doping will decrease performance, we are still able to demonstrate a relatively low-motional-impedance device using conventional semiconductor processes.

## III. Fabrication

Device fabrication was performed at the Cornell Nanoscale Science and Technology Facility (CNF), following the steps outlined in Fig. 5. Initially, a custom $n^+$ doped silicon-on-insulator (SOI) wafer with 1.3-$\mu$m-thick (100)-oriented device layer of resistivity $< 0.006\ \Omega \cdot$ cm is used. The device layer is then doped selectively using boron ion implantation to define the actuation and sensing junctions and create ohmic contacts to metal interconnects. Subsequent rapid thermal annealing is performed for dopant activation and to create the junction at the desired depth of 0.65 $\mu$m. This is followed by a reactive ion etch of the device layer to define the resonator and anchors. Interconnect and pad structures are defined by sputter deposition and wet etching of 50-nm Cr (for adhesion and to prevent spiking) and 100-nm Al. The device is released finally by HF etching.

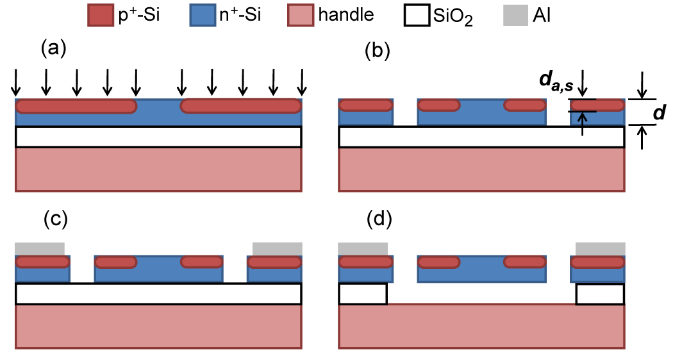


Fig. 5. (a) 1.3-$\mu$m device layer of an SOI wafer is doped selectively using boron implantation and annealed to achieve the desired junction depth of 0.65 $\mu$m. (b) Device layer is etched to define the resonator and pads. (c) Aluminum is deposited and etched to define the interconnect and pad structures. (d) Device layer is released via timed HF etch.

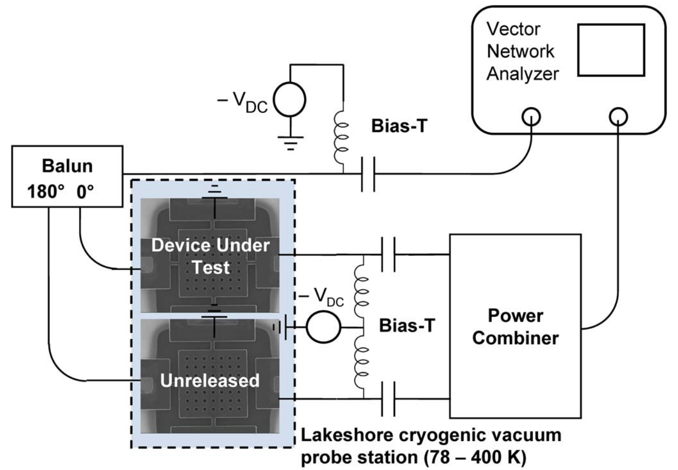


Fig. 6. Pseudodifferential measurement setup of the p-n-diode-transduced resonator to reduce capacitive loading.

## IV. Experimental Results

The experimental setup used to make the measurements of the p-n-diode resonators is shown in Fig. 6. We utilize a pseudodifferential measurement technique by simultaneously driving out of phase an identical unreleased resonator fabricated next to the device under test [16]. This is done to eliminate the loading effects of feedthrough parasitics and to measure accurately the mechanical resonance. In this case, the feedthrough path consists of the fringing field capacitance $C_{\rm ft}$ in Fig. 4 and also includes some contribution from the shunt capacitors since there is a finite impedance to ground caused by routing resistance.

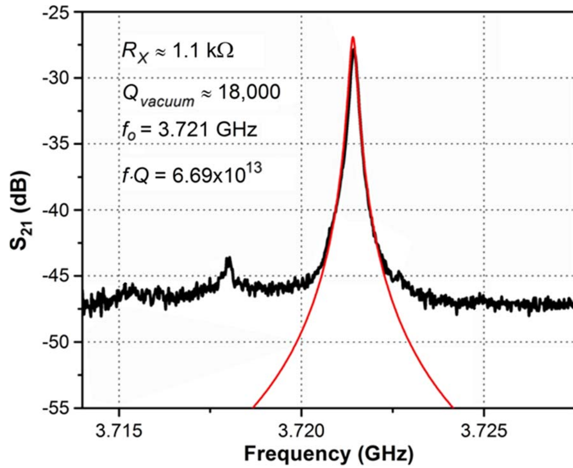


Fig. 7. Pseudodifferential transmission magnitude plot of p-n-diode-transduced resonator in vacuum demonstrating $Q \sim 18000$ at 3.72 GHz. The red trace shows that it fit with the equivalent circuit model in Fig. 4. A bias voltage of $V_{\mathrm{DC}} = -5$ V is applied to each junction.

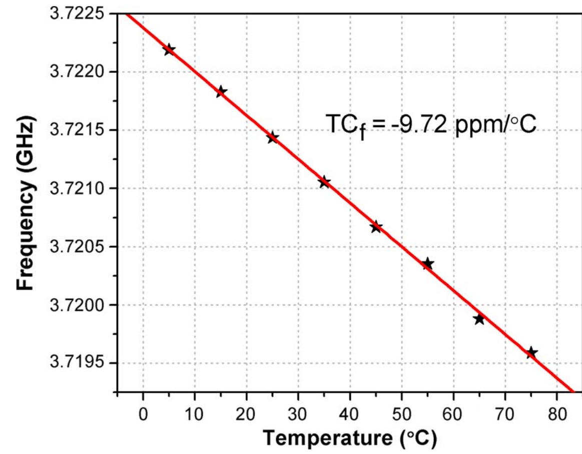


Fig. 8. Resonant frequency as a function of temperature. This figure shows linear dependence with a temperature coefficient of $-9.72$ ppm/°C over a temperature range of 5°C–75 °C.

The transmission magnitude is shown in Fig. 7, indicating a mechanical quality factor of approximately 18 000 in vacuum for the fundamental mode. The motional impedance of this particular device is 1.1 kΩ and the $f \cdot Q$ product is $6.69 \times 10^{13}$ Hz. Other than the device featured in this figure, we have measured successfully at least six other resonators, all demonstrating $R_X < 3$ kΩ and $Q > 17500$, highlighting the robustness of the proposed resonator to process variations. For these seven resonators, the frequency spread was about 24 MHz with an average frequency of roughly 3.718 GHz, indicating a 0.65% spread in the resonant frequency across devices. This can be improved by using SOI wafers with tighter device-layer-thickness tolerances. The overlaid curve in Fig. 7 is the transmission response predicted using the equivalent circuit model shown in Fig. 4. A few parameters were allowed to vary in order to fit the data, particularly the device layer thickness and doping concentration. However, the values used were well within the specified manufacturer tolerances for the device layer thickness ($\pm 0.5\ \mu$m) and the fabrication tolerances for the tools in the CNF.

We have also performed temperature measurements ranging from 5 °C to 75 °C to determine the temperature sensitivity of the p-n-diode-transduced resonators. Fig. 8 shows that the temperature coefficient of frequency $TC_f$ in this temperature range is $-9.72$ ppm/°C, which is about a factor of 3 lower than that of typical silicon micromechanical resonators. This can be attributed largely to the effect of degenerated doping on the elastic constants of semiconductors, as discussed in [17].

Fig. 9 shows a plot of the $f \cdot Q$ product of previously published high-$Q$ electrostatically transduced micromechanical resonators in addition to that of this paper. The theoretical limit predicted by phonon–phonon dissipation [18] is indicated by the black curve, showing that this paper approaches this limit. The resulting $f \cdot Q$ product is the highest ever reported in a silicon micromechanical resonator to date.

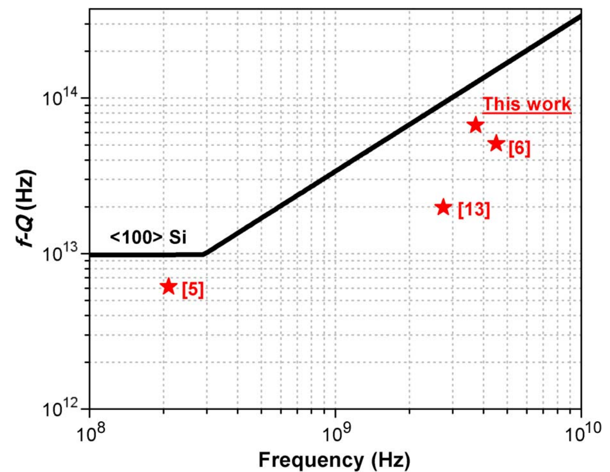


Fig. 9. The $f \cdot Q$ product of previously published high-$Q$ micromechanical resonators shown in comparison with the theoretical limit for phonon–phonon scattering in (100)-Si (black line) in [18]. This paper results in a value of $6.69 \times 10^{13}$ Hz, which is approximately half of the theoretical value at 3.72 GHz.

## V. Conclusion

We have presented in this paper a new method of transduction for micromechanical resonators, which uses the electrostatic forces in the depletion region of p-n diodes. This method combines the frequency-scaling benefits of internal dielectric transduction as well as the possible high quality factor by using a homogeneous single-crystal-silicon resonator structure. We have presented the theory of operation for such resonators and derived expressions for the equivalent BVD model in order to simplify oscillator and filter designs using these devices. Our results show a record-setting $f \cdot Q$ product in (100)-Si at room temperature of $6.69 \times 10^{13}$ Hz and indicates that on-chip integration of extremely high-$Q$ high-frequency passive components may be possible for demanding applications including transceiver local oscillator generation and narrowband filters.


## Acknowledgment

The authors would like to thank Dr. R. Polcawich at Army Research Labs and the CNF staff for their assistance in device fabrication.

## References


[1] H. C. Nathanson, W. E. Newell, R. A. Wickstrom, and J. R. Davis, Jr., "The resonant gate transistor," *IEEE Trans. Electron Devices*, vol. ED-14, no. 3, pp. 117–133, Mar. 1967.

[2] R. T. Howe and K. J. Gabriel, "Silicon micromechanics: Sensors and actuators on a chip," *IEEE Spectr.*, vol. 27, no. 7, pp. 29–31, Jul. 1990.

[3] F. D. Bannon, J. R. Clark, and C. T.-C. Nguyen, "High $Q$ HF micromechanical filters," *IEEE J. Solid-State Circuits*, vol. 35, no. 4, pp. 512–526, Apr. 2000.

[4] J. Wang, Z. Ren, and C. T.-C. Nguyen, "1.156-GHz self-aligned vibrating micromechanical disk resonator," *IEEE Trans. Ultrason. Ferroelectr. Freq. Control*, vol. 51, no. 12, pp. 1607–1628, Dec. 2004.

[5] S. Pourkamali, G. K. Ho, and F. Ayazi, "Vertical capacitive SiBARs," in *Proc. 18th IEEE Int. Conf. Micro Electro Mech. Syst. Tech. Dig.*, Miami, FL, Jan. 30–Feb. 3, 2005, pp. 211–214.

[6] D. Weinstein and S. A. Bhave, "Internal dielectric transduction in bulk mode resonators," *IEEE/ASME J. Microelectromech. Syst.*, vol. 18, no. 6, pp. 1401–1408, Dec. 2009.

[7] M. Rinaldi, B. Duick, C. Zuniga, C. Zuo, and G. Piazza, "SS-DNA functionalized ultra-thin-film AlN contour-mode with self-sustained oscillator for volatile organic chemical detection," in *Proc. 23rd IEEE Int. Conf. Micro Electro Mech. Syst. Tech. Dig.*, Hong Kong, Jan. 24–28, 2010, pp. 132–135.

[8] V. Kaajakari, T. Mattila, A. Oja, J. Kiihamaki, and H. Seppa, "Square-extensional mode single-crystal silicon micromechanical resonator for low-phase-noise oscillator applications," *IEEE Electron Device Lett.*, vol. 25, no. 4, pp. 173–175, Apr. 2004.

[9] T. Cheng and S. A. Bhave, "High-Q, low impedance polysilicon resonators with 10 nm air gaps," in *Proc. 23rd IEEE Int. Conf. Micro Electro Mech. Syst. Tech. Dig.*, Hong Kong, Jan. 24–28, 2010, pp. 695–698.

[10] L.-W. Hung, Z. A. Jacobson, Z. Ren, A. Javey, and C. T.-C. Nguyen, "Capacitive transducer strengthening via ALD-enabled partial gap filling," in *Proc. Solid State Sens., Actuators, Microsyst. Workshop Tech. Dig.*, Hilton Head Island, SC, Jun. 1–5, 2008, pp. 208–211.

[11] G. Piazza, P. J. Stephanou, and A. P. Pisano, "Piezoelectric aluminum nitride vibrating contour-mode MEMS resonators," *IEEE/ASME J. Microelectromech. Syst.*, vol. 15, no. 6, pp. 1406–1418, Dec. 2006.

[12] H. Chandrahalim, D. Weinstein, L. F. Cheow, and S. A. Bhave, "High-K dielectrically transduced MEMS thickness shear mode resonators and tunable channel-select RF filters," *Sens. Actuators A, Phys.*, vol. 136, no. 2, pp. 527–539, May 2007.

[13] M. Ziaei-Moayyed, E. P. Quevy, J. Hsieh, and R. T. Howe, "Efficient internal electrostatic transduction of the 41st radial mode of a ring resonator," in *Proc. 23rd IEEE Int. Conf. Micro Electro Mech. Syst. Tech. Dig.*, Hong Kong, Jan. 24–28, 2010, pp. 711–714.

[14] J. H. T. Ransley, C. Durkin, and A. A. Seshia, "A depletion layer actuator," in *Proc. 14th Int. Conf. Sens., Actuators, Microsyst.*, Lyon, France, Jun. 10–14, 2007, pp. 1393–1396.

[15] S. W. P. van Sterkenburg, "The electrostriction of silicon and diamond," *J. Phys. D, Appl. Phys.*, vol. 25, no. 6, pp. 996–1003, Jun. 1992.

[16] J. E.-Y. Lee and A. A. Seshia, "Parasitic feedthrough cancellation techniques for enhanced electrical characterization of electrostatic microresonators," *Sens. Actuators A, Phys.*, vol. 156, no. 1, pp. 36–42, Nov. 2009.

[17] A. K. Samarao and F. Ayazi, "Temperature compensation of silicon micromechanical resonators via degenerate doping," in *IEDM Tech. Dig.*, Balitmore, MD, 2009, pp. 789–792.

[18] R. Tabrizian, M. Rais-Zadeh, and F. Ayazi, "Effect of phonon interactions on limiting the $f \cdot Q$ product of micromechanical resonators," in *Proc. 15th Int. Conf. Sens., Actuators, Microsyst.*, Denver, CO, Jun. 21–25, 2009, pp. 2131–2134.

**Eugene Hwang** (S'06) received the B.S. degree in electrical engineering and computer science from the University of California, Berkeley, in 2006. He is currently working toward the Ph.D. degree in electrical and computer engineering with Cornell University, Ithaca, NY.

His research interests include low-power RF and analog circuit design; micromechanical systems for RF applications, acoustics, and ultrasonics; microelectromechanical systems–complementary metal–oxide–semiconductor integration; and nonlinear dynamics in micro- and nanoscale devices.

**Sunil A. Bhave** (S'99–M'04–SM'10) received the B.S. and Ph.D. degrees in electrical engineering and computer sciences from the University of California, Berkeley, in 1998 and 2004, respectively.

Since October 2004, he has been with Cornell University, Ithaca, NY, where he is currently an Associate Professor with the School of Electrical and Computer Engineering. His research interests include microelectromechanical resonators for radio front ends, merged complementary metal–oxide–semiconductor and nanoelectromechanical systems (NEMS) for low-power computation, inertial and acoustic sensors, and hybrid photonic NEMS and magnetic NEMS for low-phase-noise microwave oscillators.

Dr. Bhave was a recipient of the National Science Foundation Early CAREER Development Award in 2007 and the Defense Advanced Research Projects Agency Young Faculty Award in 2008. Along with his students, he has been awarded the Roger A. Hakan Best Paper Award at International Electron Devices Meeting 2007 and is the winner of the Student Paper Competition at the 2009 IEEE International Ultrasonics Symposium.